Artifact Authentication and Characterization

Prepared By:

Rachel Ellen Handel

Faculty Advisors:

Dr. Michael West
REU Site Director, Department Head Materials and Metallurgical Engineering

Dr. William Cross
Associate Professor, Department of Materials and Metallurgical Engineering

Dr. Alfred Boysen
Professor, Department of Humanities

Table of Contents

Abstract

An artifact of questionable authenticity was studied at length using micro computed tomography, scanning electron microscopy, and optical microscopy in order to verify its age and make. Analysis was conducted so that samples of the artifact were evaluated by each method, making certain that the individual results can supplement one another. Scientific results were coupled with a significant amount of research on forgeries, as well as the history of metallurgy and the Middle East, in order to conclude that the artifact is neither Mesopotamian nor 3200 years old.

Introduction

Background

The role of materials in the progression of mankind has been significant enough to define time periods as a function of the primary crafting material used. Subsequently, man has passed from the Stone Age through the Copper, Bronze, and Iron Ages to where it is today, in somewhat of a Polymer/ Advanced Alloy Age.

Within the confines of this paper, the Near East will be examined in detail to evaluate historical data known about the production and usage of ancient materials. Via the authentication and characterization of a Mesopotamian artifact, analysis of this geographical region will be restricted to the Late Bronze Age, its trading patterns, available metal ores, and ability to metalwork bronze.

Objectives

The artifact, shown in Figures 1a and 1b, is a lion with a loop near the top middle suggesting that it was meant to be hung. Facial features can be clearly seen, including a snout, ears, and eye indentations.

Figures 1a and 1b: Two images of the lion after the outermost layer of corrosion has been removed, revealing a darker thicker corrosion layer underneath.

The artifact, as purchased from Sadigh Gallery, comes with a certificate of authenticity pictured in Figure 2.
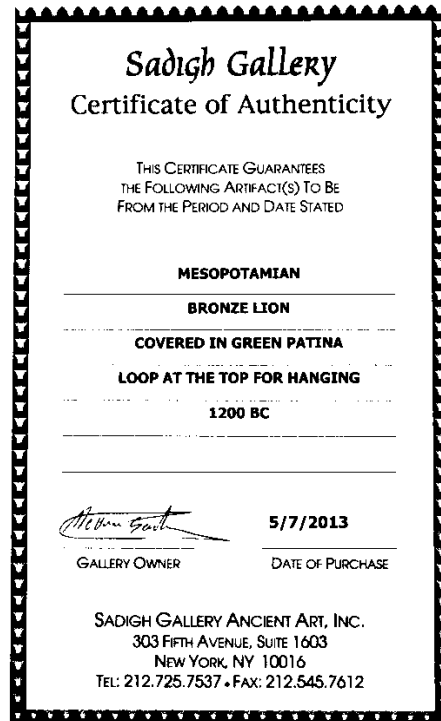

Figure 2: Certificate of Authenticity, as signed by the Gallery Owner

The certificate guarantees three main points:

1. The lion is bronze.

2. The lion is Mesopotamian.

3. The lion is from 1200 BC.

In this study several analytical techniques will be used to confirm these stipulations and authenticate the artifact.

Developmental Plan

Several analytical techniques will be used to expose the lion's physical and chemical properties.

Micro computed tomography (microCT) constructs a 3D image of the internal structure of an object, much like a medical CAT scan. It is designed with a variety of specifications in order to be able to handle materials of a variety of densities, sizes, and thicknesses. It works by rotating the mounted sample in tiny increments (less than 1 degree) through approximately 180 degrees and taking detailed images at every angle. These images are then reconstructed into a 3D model that can be manipulated using the computer software Avizo to generate a color scale based on different densities within the inner structure of the material. This allows us to nondestructively visualize the inner contents of the lion to evaluate methods by which it could have been made, depending on the prevalence or lack of defects. This also provides a starting point for future operations, accurately highlighting interest areas that should later be bisected or tested at a higher magnification.

The microCT has been used sparsely in past archaeometallurgical studies to nondestructively, noninvasively analyze small metal antiquities. There are many advantages to the procedure beyond the physical preservation of the artifact; the test on low magnifications is an excellent

way to visualize an entire inner structure of a small metal object. From there the test can then be honed in on specific sections of the object to study defects or inconsistencies in detail. After the 3D image is produced, it can be sent to Avizo which treats the image like a CAD file and will allow you to look at it from any direction, cross section, or data range.

Disadvantages of the procedure include its long run time for a good image; this can take more than 12 hours. In addition, the images taken at high magnification can be difficult to assemble into one large, high resolution image. Avizo is a toilsome program with a long handbook.

Most popularly, the microCT has been used to provide information about mummies. Researchers were able to nondestructively, noninvasively determine the sex, approximate age, and a possible cause of death of some Egyptian mummies, such as Jeni who may have been run over by a chariot[7]. Additionally, they were able to study how the body was processed after death to reveal emptying of the cranium via the nose and individual packaging of internal organs. All of this was done without disturbing the body. Using the microCT to characterize ancient *metal* artifacts is a relatively new thing. In recently published journal articles, the microCT has been used to visualize degrading glass unable to be extracted from soil[8] or to detect repairs made on old bronze objects [4], but neither of these studies combine this method with other techniques as will be shown in this paper.

The SEM shoots a beam of electrons onto a specimen. When the electrons come into contact with atoms on the surface of the material, they can do two different things. They can replace electrons in the outer shell of the atom, generating secondary electrons (SE). The atom's original electrons are then liberated, giving off a quantifiable amount of energy. Detectors positioned within the SEM pick up the SE signal and the amount of energy they create in the form of x-rays.

Second, if the electron beam bounces directly back off of the sample surface, the SEM has a backscatter (AsB) function that allows it to pick up these x-ray energies to show differences in the mass of elements. Heavier elements will give off higher energy x-rays and will be shown as brighter spots.

The SEM has many distinct advantages over older testing technologies, some of which must be taken with a grain of salt. The samples needed for analysis can be very tiny; most features can be visible with certainty down to about 50 nanometers. It is when the surface of the sample begins to vary in texture that the image has a higher deviation. Because of the location of the detector relative to the sample surface, electrons cannot always travel in a straight line from the surface to the detector, as is the case with cavities on the surface that could better be visualized with optical microscopy. Often it is necessary to scan larger areas to obtain overall data rather than concentrating on tiny features. As a whole, however, the SEM greatly simplifies the material identification process and provides a standard for this communication across all of research. The SEM has not been extensively utilized in the field of archaeometallurgy because it often requires the sample to be cut apart and, at times, polished. When this does become a feasible action, the SEM has been used to study the corrosion of artifacts in detail. Specifically, a 2010 paper compared a few pieces found near Lake Van from the 1st century BC to investigate effects of soil on the corrosion mechanism. The pieces were buried at different depths, exhibiting that an item closer to ground level will be more affected by humidity and a different salt content[1].

Optical microscopy is used to visualize the surface of a material, revealing grain boundaries, sizes, and orientations. In order to figure out the make of a piece of ancient material, it is practical to study the arrangement of these things. Large irregular grains indicate a cast object. Grains that are misshapen or pattern in certain ways have likely been worked. In order to show

these features the sample must be etched, which will make grain boundaries visible by selectively destroying them. Different etchants are meant to bring out different features in the material.

Optical microscopy can be an excellent resource to visualize the microstructure of a metal with low maintenance costs and a small time investment, however it cannot obtain detailed images at high magnifications like an SEM. Other problems can be associated with sample preparation. For example, if a sample is not finely polished scratches will mar the surface and prevent features from being readily distinguishable. Additionally, a proper etchant must be selected and correctly applied.

Optical microscopy (OM) has been used similarly to scanning electron microscopy, often the two resources are paired together to thoroughly analyze one site. It has been used in archaeometallurgy to evaluate the ability of metalsmiths to cast, forge, and repair metals. For example, OM contributed to a study of Nubian solder joints found in a mirror, ladle, and two bronze bowls, showing structural changes over time and phases of the material[5].

It is worth mentioning that these methods are destructive. This artifact, when purchased, was of questionable authenticity and has been sacrificed in the name of science to aid future investigations of Bronze Age metalwork. Figure 3 shows the sites that are used in headings later.
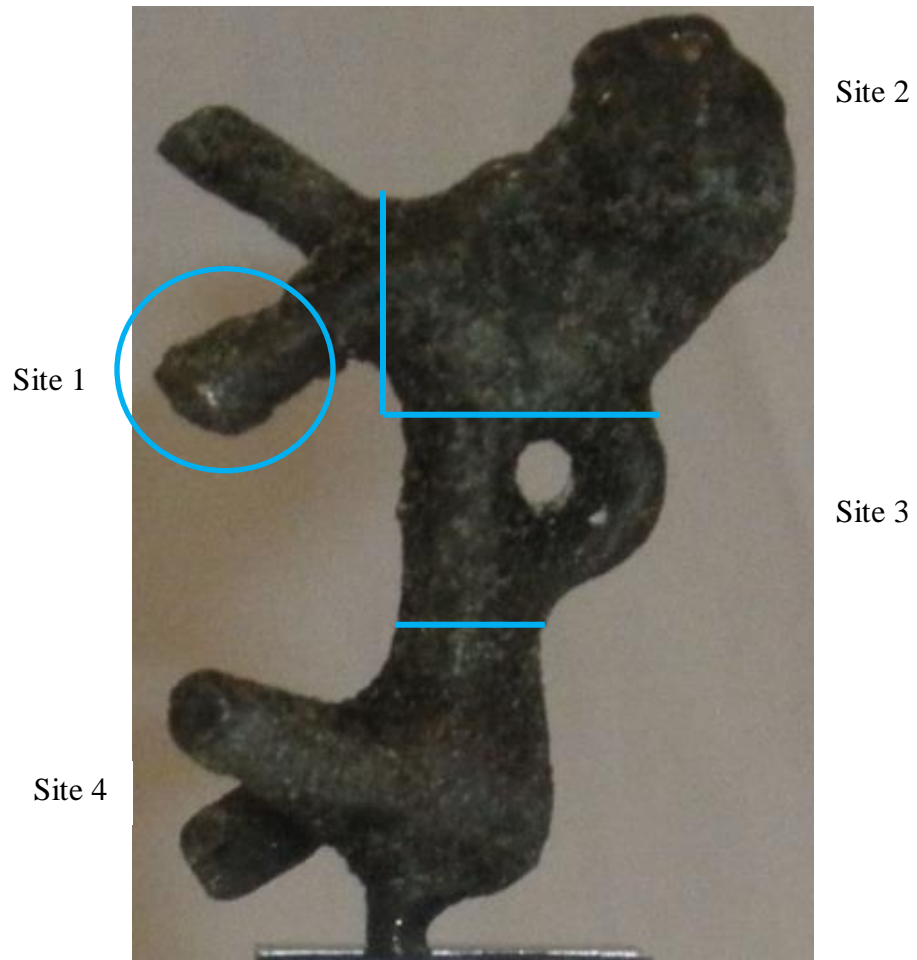
Figure 3: Destructive Testing Locations

Historical Context

The future of archaeometallurgy looks chaotic at best, considering newly emerging technologies and the rise of information dispersal. Several methods of study are highly controversial, including the interpretive lead isotope testing[9] and invasive tests that can't preserve the integrity of the original artifact. Even more problematic are black market goods and the propensity for people to forge antiquities to make quick buck. The key is to find a balance that can preserve the dignity of the material, but still allow us to reveal its story (whether it is what you expected or not).

Decorations and jewelry used to be delicacies reserved only for the upper class, the lower class left to a lifetime of wanting. With the emergence of the middle class people began to bridge the gap and have a minimal amount of surplus funds. As such, makers expanding their customer base were forced to find new ways to produce valuable baubles at a fraction of the cost. Thus emerged the art of forgery[3]!

Consider that, at the South Dakota School of Mines and Technology (SDSM&T), while this project was being conducted, we were able to reproduce several castings of the lion very easily and quickly as shown below in Figure 4.

Figure 4: Five figures produced at SDSM&T and the darker, corroded original copy

To make the copies, a spin mold of the original was made using clay and silicone; the copies are made of tin and exhibit high levels of detail as seen on the original piece. (When synthetic materials replaced plaster in the 1950's the amount of detail transfer drastically increased, making for more accurate replicas[3].) There was a minor amount of flashing that could be taken off with a small knife. Additionally, impurities within the tin segregated to the top of the lions resulting in a yellow appearance.

Other ways of making three dimensional copies include the less accurate but more historically popular pointing method as has been used for hundreds of years across the globe, especially with Roman copies of Greek stone statues. Digital scanning has replaced pointing in modern times, where a 3D surface is essentially photographed and copied[3].

After the lion was cast using any of these aforementioned methods, the trick is to get it to *look* like it's 3200 years old. There exist many artificial corrosion environments that can carefully alter the outside of an artifact to change its color, texture, and chemical composition. In the 1900s the use of skillful, time consuming patination began to decline as simpler techniques only required a chemical bath, spray coating, or electrolysis. Most chemical treatments involve sulfur, nitrogen, or chlorine in some combination with copper[3].

Procedure

Part 1: MicroCT

Attached in Appendix 1 is a step by step procedure used with the Xradia XCT 400, a micro X-ray computed tomography machine. As show below in Figures 5a and 5b, the microCT positions the sample on a mount in between the source (left) and the detector (right).

S   D
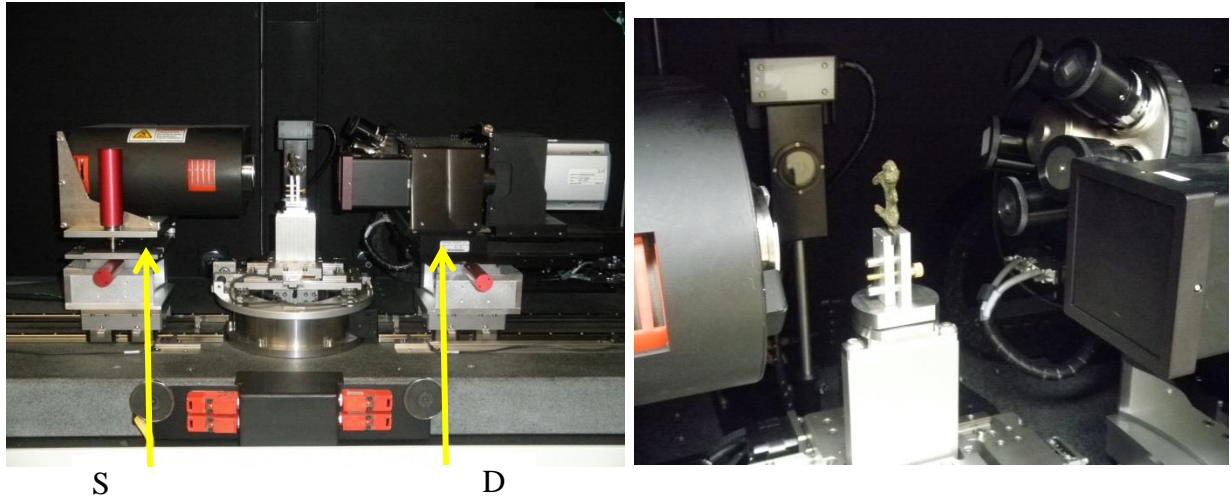
Figures 5a and 5b: Inside the microCT with sample mounted vertically by tail showing source (S) and detector (D)

This artifact is a thick, dense sample that requires high energy x-rays to properly visualize its internal features. Several variables, as indicated below in Table 1, make this possible.

Table 1: MicroCT variables

	Focus	Voltage (kV)	Filter	Time (s)	Number of Images	Binning	a/b Count	Pixel Size	Magnification
Trial 1	Whole body #1	140	HE #5	10	1600	2	N/A	~45µm	0.39x
Trial 2	Head	150	HE #6	30	1600	2	N/A	~18µm	1x
Trial 3	Neck	150	HE #6	30	1600	2	N/A	~18µm	1x
Trial 4	Back Leg Junction	150	HE #6	30	1600	2	0.01-0.03	~18µm	1x
Trial 5	Whole Body #2	140	He #5	10	1600	2	N/A	~45µm	0.39x

The voltage of the machine can run at any setting from 40-150 kV when combined with the proper filter. The filters are designed to focus X-ray penetration by varying the sampling rate of the detector. Two other important variables that will crucially impact the quality of the final projection are the exposure time and the number of images. A longer time lets more energy pass through the sample. For trials of the whole lion body, a balance must be reached between the thickness of the lion and its surrounding air (so as to avoid a wash out). For these trails the time was set at only 10 seconds per image. In trials where a thick portion of the lion was being analyzed at a higher magnification (taking up the entire screen), the time was increased to 30 seconds.

The machine acquires transmission images as the object rotates in increments through approximately 180 degrees. A higher resolution image will be the result of images taken very close to one another as the subject rotates. In other words the final product will be better as the degree of change between images approaches zero. Since this is highly impractical (it would take an infinite amount of time), one must compromise; it is generally accepted that 1600 images will produce a smooth end product.

Next Avizo was used to generate some images of the sample. This software enables the user to carefully select more advanced parameters than the microCT machine will.

These microCT trials will show the internal features of the lion. It was expected that if the lion is 3200 years old there will be some defects that will tell us more about how the lion was made and the skill of the metalsmiths. The thickness and layers of corrosion on the outside of the lion should also be visualized.

Part 2: Scanning Electron Microscope with Energy Dispersive Spectroscopy

The front left leg of the lion was cut using a jeweler's saw and cold mounted in epoxy to prevent the sample from having a heat treated zone. The surface of the sample was polished to 1 micron in order to clearly show the outside layers of corrosion. The first sample was then coated in carbon to ensure that portions will not build up a charge. Other samples (see Figure 3) were prepared similarly, but only required the use of carbon tape instead of a coating. The samples were evaluated in a Zeiss Supra 40 VP Scanning Electron Microscope shown below in Figure 6.
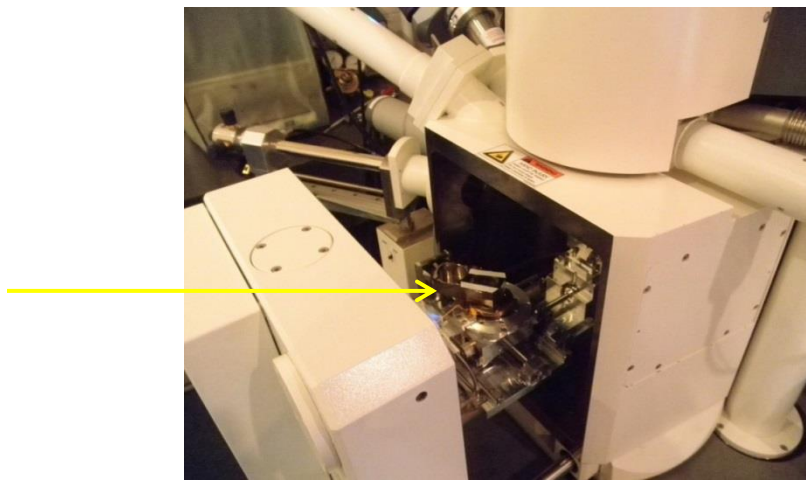
Figure 6: Sample mounted in the SEM with carbon tape (white) on either side to ensure the sample will not charge

Within the SEM program several critical factors must be taken into account, as listed below:

- The focus set at 8.5mm

- High current selected

- Aperature size increased to 60 micrometers

- Two detectors used: SE2 and AsB

Images were then analyzed using Aztec's energy dispersive spectroscopy (EDS) software to analyze sample composition. Three different functions were used: mapping, point, and area analyses.

It was expected that the SEM with EDS will provide a quantitative chemical composition for the samples. With this we can compare historical research about popular Late Bronze Age metal compositions to authenticate the artifact's place and age of origin. Additionally, the different map and point functions on the SEM show changes in composition throughout the material, including impurities and different phases.

Part 3: Optical Microscope

After the sample was prepared for the SEM, the carbon coating (only applied to sample 1) had to be polished off and refined to 1 micron in order to etch for OM. The etchant selected was the most common type listed in *Metallography Principles and Practice:* a mixture of equal parts ammonium hydroxide, 3% peroxide, and water. The etchant was swabbed to remove surface accumulations that a simple immersion would not accomplish.

The samples were evaluated on a Nikon Epiphot 200 which has an automatic lighting feature and magnifications ranging from 50X to 1000X.

Figure 7: Optical Microscope with mounted sample

From the OM information about the microstructure(s) of the metal will be revealed, which can tell us more about the processing of the metal and how the constituents interact.

Part 4: X-Ray Fluorescence

To verify the chemical composition of the specimen, Sites 2 and 4 were evaluated using a Bruker

Tracer IV-SD x-ray fluorescence machine. It operates by hitting the specimen with high energy

x-rays and then measuring the energy given off. Samples do not have to be prepared, thus it is a

nondestructive, noninvasive test method.

Results

MicroCT

The images below are two scans taken of the entire lion at 0.39X. Figure 8a shows an outer layer of corrosion (less dense material) surrounding the lion like an outer skeleton. Areas of bright orange are the most dense, while spaces trending to dark blue appear to be the least dense. This is probably the result of a casting flaw in the thickest part of the material. These are seen in two places, the neck and the hind leg junction. At this point it cannot be determined if this is the result of a large cavity or many smaller pores. It is thought that the sample is solid metal however, because these areas would be wholly black if they contained some sort of other material like plaster or clay.

Figure 8b is from Avizo and shows a transcluscent outer shell of the lion constructed by selecting a limited range of data that will display specific density values. The dark neck area in Figure 8a can be more closely explored here; it appears to have a v shape wandering from the outside of the neck into the head and middle neck region.
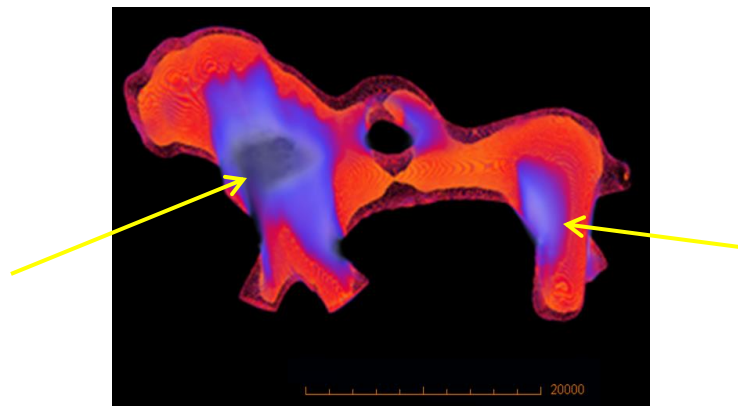
Figure 8a: Whole body scan of lion, showing regions of different density
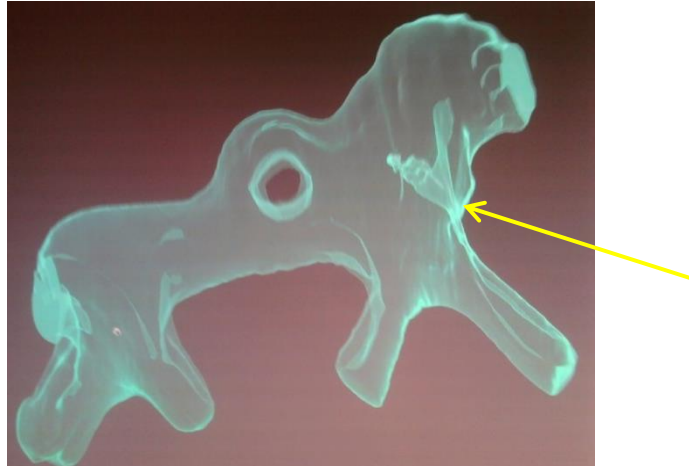
Figure 8b: Whole body scan of lion as generated by Avizo, showing outer surface

Below are two figures taken at 1X showing detailed features of the lion. Figure 9a shows details on the head where there appear to be vestiges of eyes, a snout, and a mouth. Figure 9b displays a close up image of the possible cavity seen in Figure 8a on top of the hind legs of the lion.
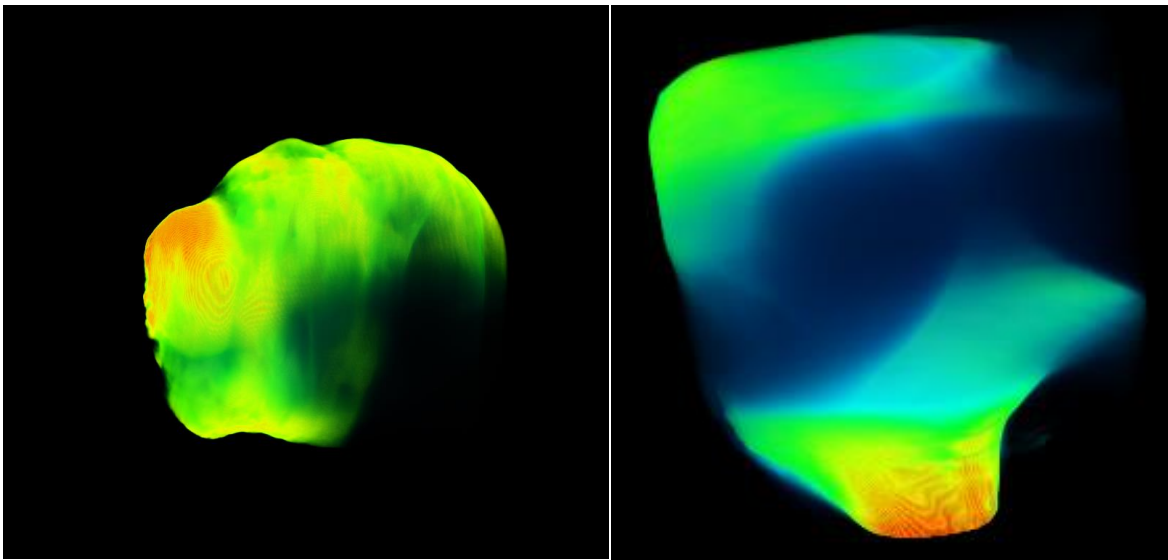
Figures 9a and 9b: Head of lion showing facial features (snout is red), hind region of lion showing less dense area in navy blue

Mold Making Process

During the casting procedure referenced in the introduction, an outer layer of corrosion was

removed when the lion was coated with clay, as shown below in Figure 10. It revealed a dark

brown/ black layer underneath the original dark green color (see Figures 1a and 1b).

Figure 10: Clay mold of the lion, light brown corrosion layer visible especially on the lion's rear

Site 1: SEM

Figure11 below shows a map of the bulk material using the AZtec EDS software on Site 1. Lead

does not dissolve in copper, as it is shown below to have evenly distributed in chunks throughout

the sample.
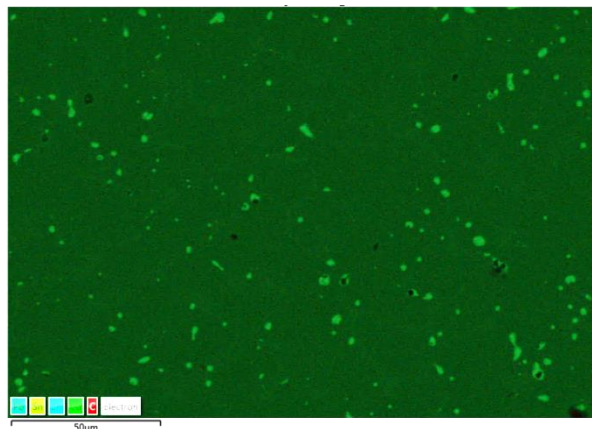
Figure 11: Site 1 bulk material distribution, showing lead globules (bright green) throughout
copper-zinc matrix (dark green)

Figure 12, below, provides a quantitative summary of the compositions seen in this bulk material

scan. The table in the top right corner indicates that the material is in fact brass, not bronze,

containing 31.0 wt% zinc (30.7 at%). Additionally, there is a significant quantity of lead. By

modern definition, this makes the material a leaded yellow brass. The amount of aluminum can

mostly (if not wholly) be attributed to the 1 micron polishing agent, alumina alpha c suspended

in distilled water.
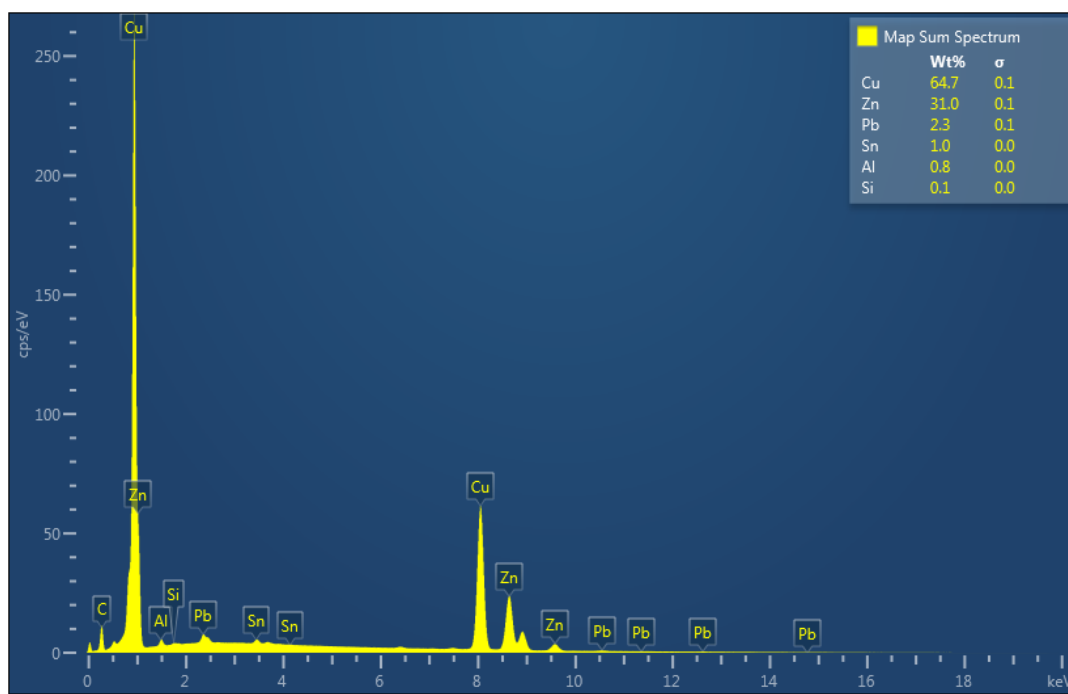
Figure 12: Peaks from a Map Sum Spectrum conducted in the middle of Site 1

Figures 13a, 13b, and 13c below show the results of individual element maps of Site 1. Copper

and zinc appear to be evenly distributed throughout the material, except where lead is

concentrated.

Cu Kα1   Zn Kα1

50μm   50μm
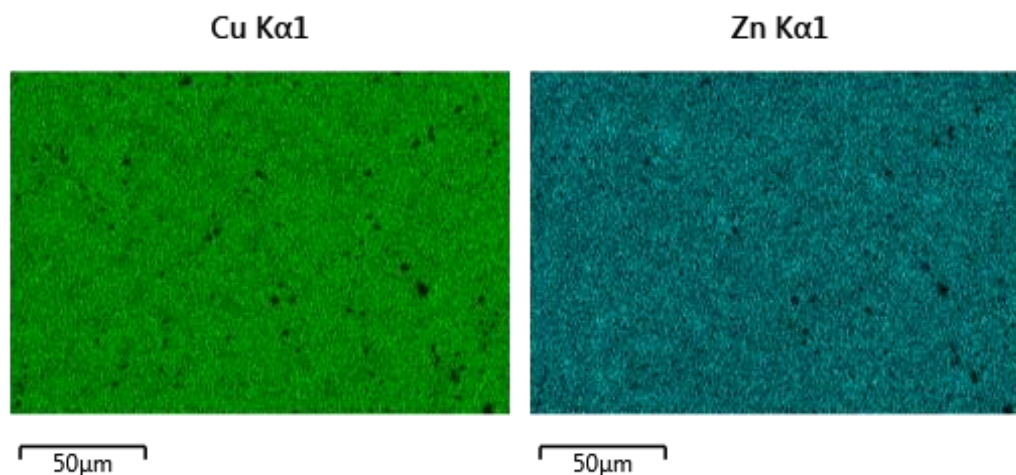
Figure 13a: Copper distribution in green   Figure 13b: Zinc distribution in blue

Pb Mα1

50μm
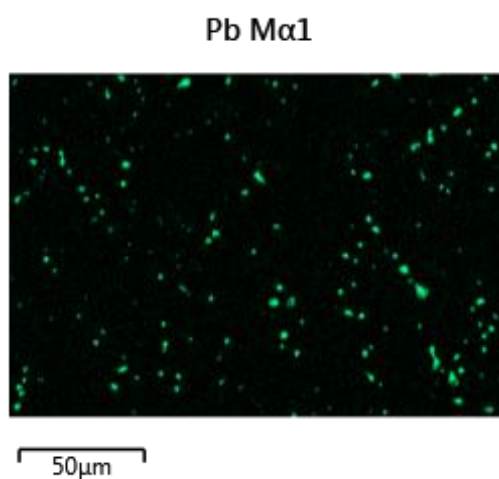
Figure 13c: Clumps of dense, concentrated lead shown in fluorescent green

Next the corrosion compositions (Figure 14 below) were analyzed using EDS. There appear to

be three different layers; two corrosion layers are teal and green, while pink reflects the copper-

zinc insides. The two corrosion layers total about 25 micrometers. In this image the corrosion is

also beginning to break its way further into the bulk material as can be seen in the middle of the

image where green tendrils begin to reach into the pink region.
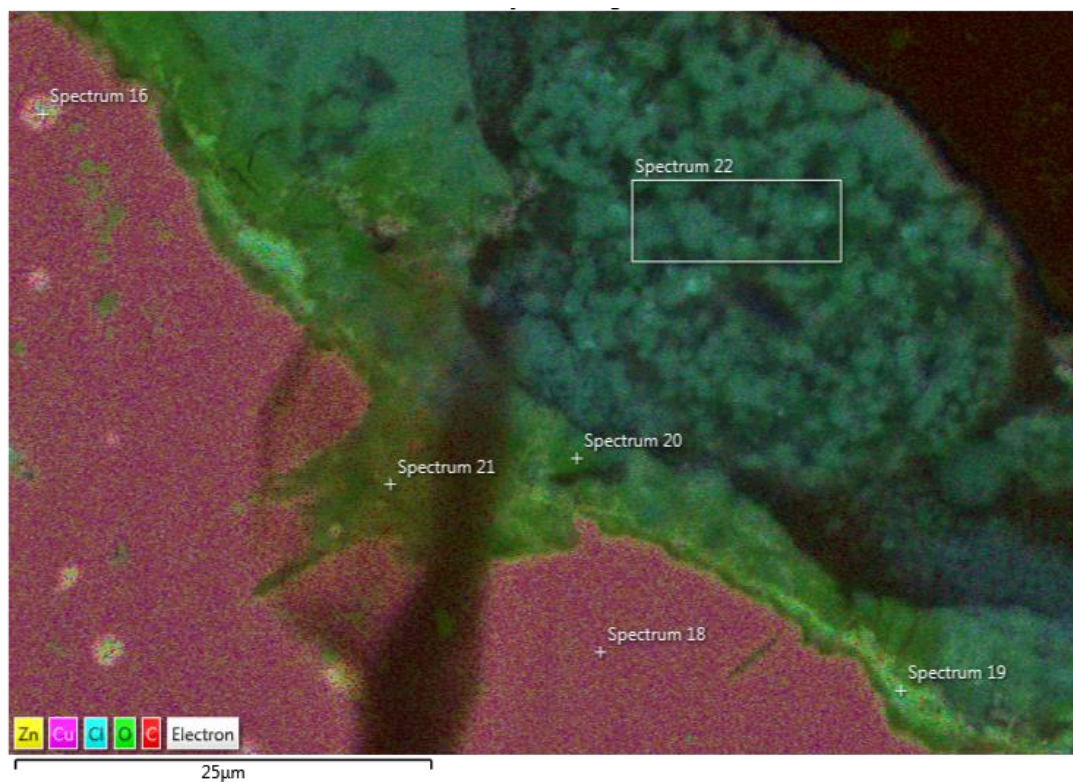
Figure 14: Three layers of material (teal, green, pink)

Table 2: Compositional totals, weight percent

	Map Sum	Spectrum 16	Spectrum 18	Spectrum 19	Spectrum 20	Spectrum 22
Cu	48.3	8.5	67.6	13.3	25.8	42.6
Zn	23.5	4.8	31.2	10.7	44.5	8
O	10.9	3.2		12.5	11.3	20.3
Cl	6.9			9.4	10.1	15.9
Pb	3.1	83.5		55.2		
Fe	1.8			0.6	0.9	6.3
Sn	1.8		0.5			4.9
Al	0.9		0.6			0.5
Ti	0.9				2	0.3
Si	0.8			0.9	0.7	0.4
S	0.6				2.9	
Ca	0.5			0.3	1.7	0.8

Table 2, above, shows the composition values obtained at each spectrum in Figure 14. The overall map sum shows that the percentage of copper has fallen from 64.7 to 48.3 wt%. The zinc content has also fallen from 31.0 to 23.5 wt%. Looking closely at "spectrum 22" there is an extremely low concentration of zinc, only 8 wt%, whereas the concentration of copper has remained more stable at 42.6 wt%.

A highly unusual presence of chlorine and iron, as much as 15.9 wt% Cl and 6.3% Fe in "spectrum 22," indicates that the specimen was probably placed in an artificial chlorinated environment to induce corrosion quickly and make the artifact look old.

Site 1: Optical Microscopy

Copper-based structures like brass and bronze look very similar under the optical microscope. The actual composition cannot be determined with OM, but can be used to affirm SEM results as used here.

Figures 15a-d are shown a series of images of increasing magnification of the brass sample. They all reveal that there are clearly two different metal phases, an alpha and beta phase. All of the samples exhibit profound dendrites (higher in copper than the surrounding area) oriented in markedly different directions, indicating how the material cooled. Beginning at the 500X image (Figure 15c) the lead globules visualized on the SEM can be seen as dark round spots.
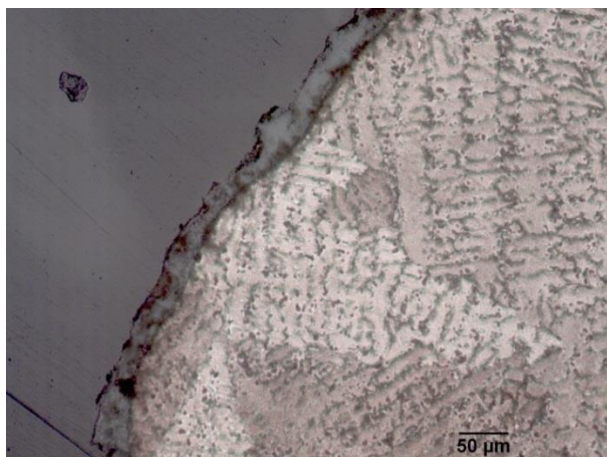
Figure 15a: 200X OM image of lion foot

Figure 15b: 200X image of lion foot
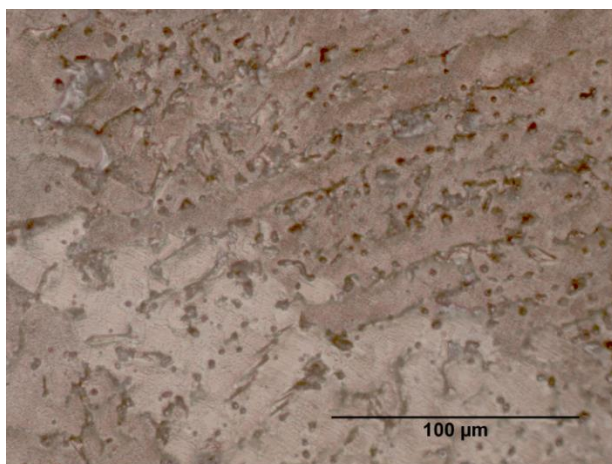
Figure 15c: 500X image of lion foot
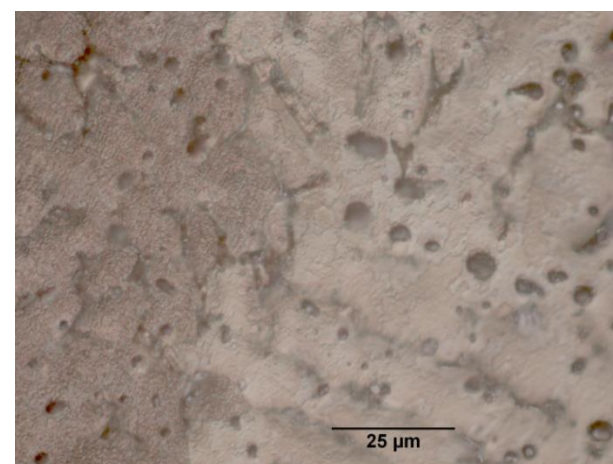
Figure 15d: 1000X image of lion foot

Site 2: SEM

A map analysis on the head verified that the high zinc composition was not a fluke in the leg, coming in at 32.2 wt% as shown in Figure 17 below. Lead is still well spread throughout the copper-zinc matrix. There is also a portion of the material significantly higher in tin than areas seen in the leg, as shown by the pink areas in Figure 16.
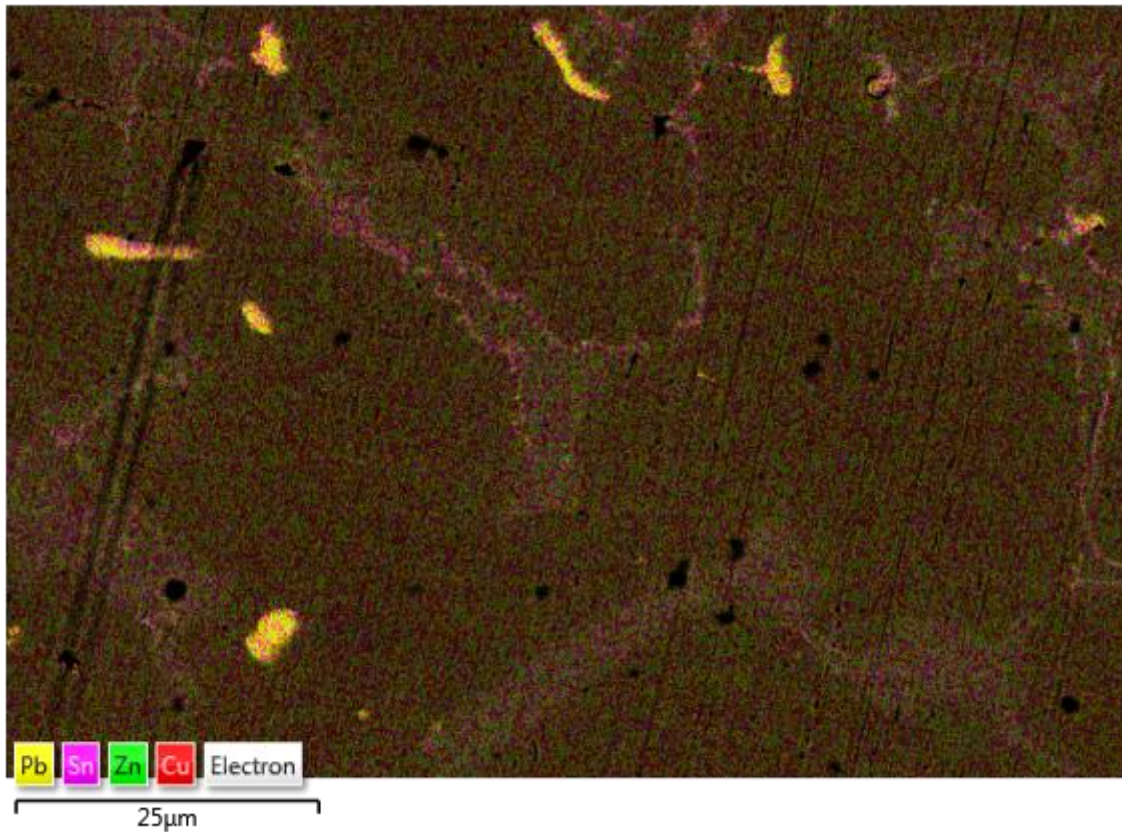
Figure 16: Layered Map of head bulk material, showing lead globules (bright yellow) as well as tendrils of tin containing brass (slight pink)
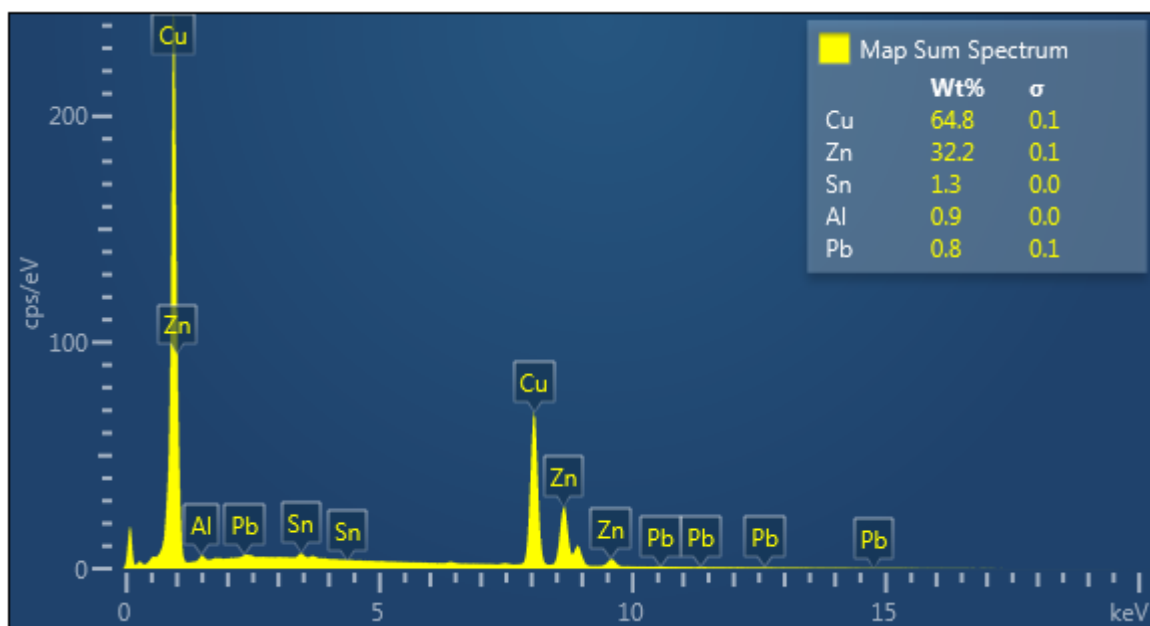
Figure 17: Compositional result of Site 2 map sum

Figure 18, below, shows a region found in the middle of the neck that contains pores. This matches up with the less dense area indicated by the microCT. The pores are oblong shaped and clustered closely together, some being more than 100 microns long.
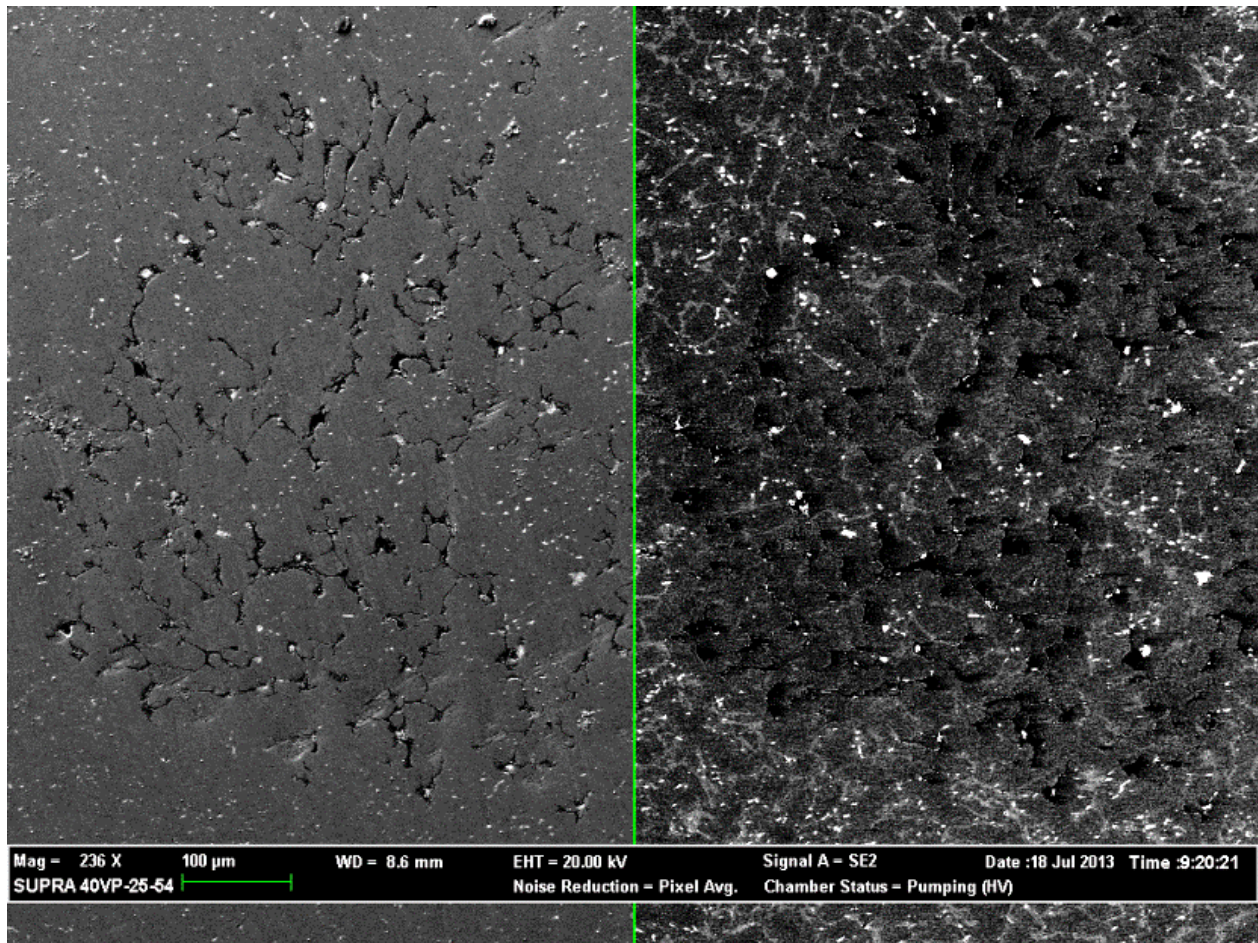
Figure 18: Head pores, shown with SE2 on left, AsB on right

Figures 19a and 19b, below, show SEM images of Site 2 after it has been etched. Grain boundaries can be clearly seen in a regular pattern throughout the material. Additionally, there appear to be two different textures on the sample, a rougher pattern with darker portions to the right and a completely smooth gray to the left.
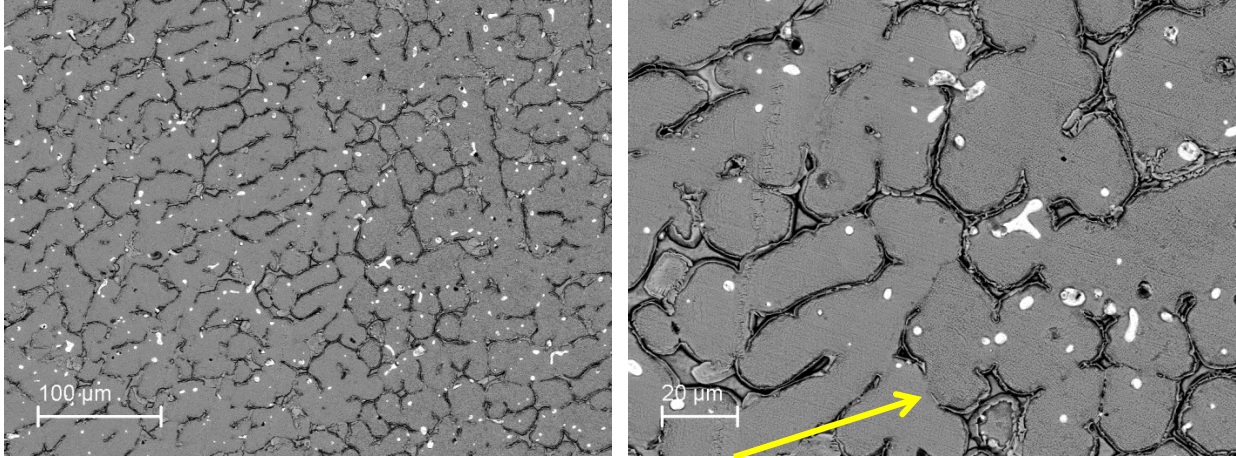
Figures 19a and 19b: Etched Site 2, showing two differently textured materials as indicated by the yellow arrow

Figure 20, below, shows a close up image of these two different textures. Different visual patterns in the material correlate with slightly different concentrations. "Spectrum 9" at the grain boundary has a noteworthy, higher tin content (6.9 wt%), implying that tin segregates to certain areas of the material. This matches with results shown in Figure 16. Other compositional results are shown below in Table 3.
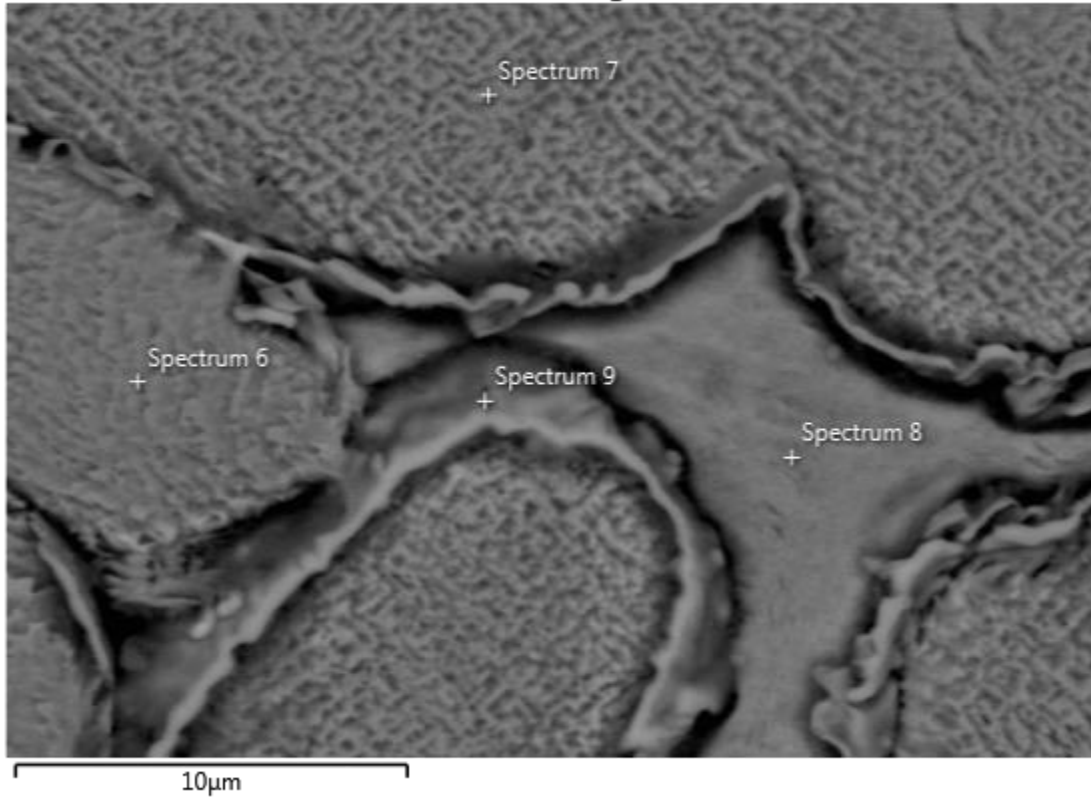
Figure 20: Etched Site 2, showing corroded grain boundaries

Table 3: Etched Site 2, weight percent

	Total	Spectrum 6	Spectrum 7	Spectrum 8	Spectrum 9
Cu	52	56	55.1	46.4	45.8
Zn	23.5	24	22.6	29.5	25.4
O	20.6	20	20.5	20.8	20.7
Sn	2.1		0.4	2.1	6.9
Al	0.5		0.4	0.7	0.7
Si	0.5		0.4	0.6	0.4
Fe	0.4		0.4		
Pb	0.3				

Site 2: Optical Microscopy

Optical microscopy on Site 2 showed essentially the same features that were seen in Site 1.

Figure 21a displays dendritic action in a more irregular, less linear fashion. This could be due to

the thickness of the casting at this location and because the head of the lion would be able to cool

from all directions. Figure 21b shows pores seen on the SEM and in the microCT.
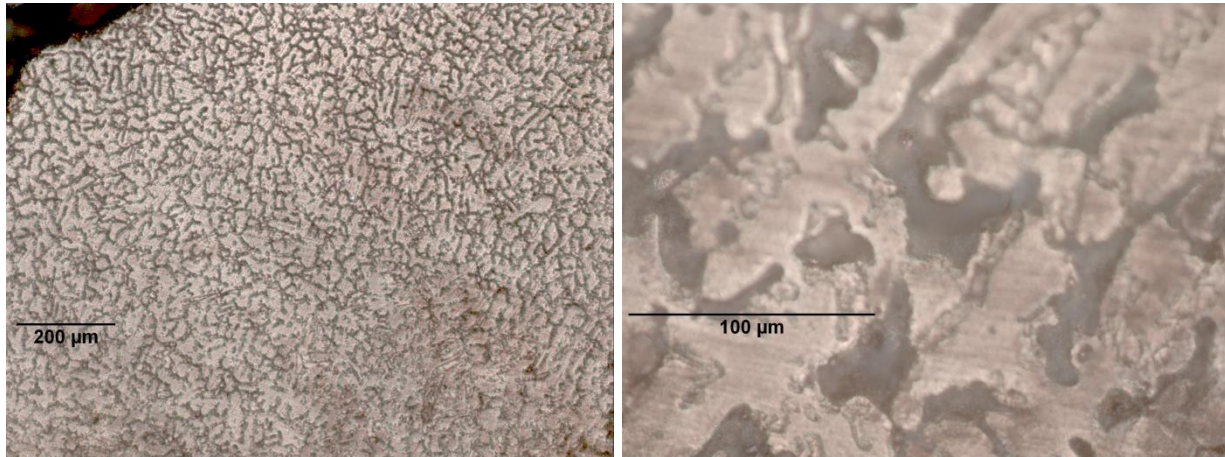
Figures 21a and 21b: Optical microscopy of head at 100X (left) and 500X (right)

Site 3: SEM

SEM EDS data from Site 3 shows the bulk material composition to be near the compositions of

the other samples, measured at 64.8 wt% copper and 30.8 wt% zinc as shown in Figure 22b.
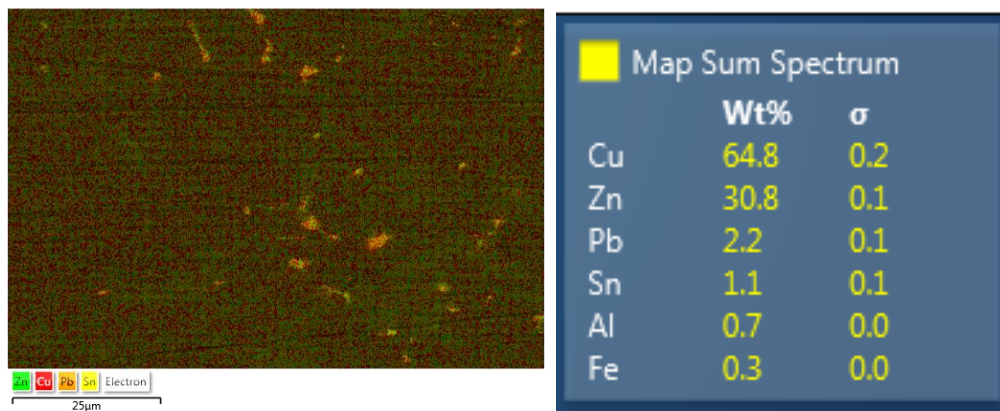
Figures 22a and 22b: EDS data of bulk material of Site 3

Site 3: Optical Microscopy

Site 3 is one of the thinnest (quickest cooling) parts of the material. It shows stunning linear

dendrites in both alpha and beta phases (Figure 23a). Figure 23b shows a transition area where

Site 3 gradually gets nearer to Site 2 and the dendrites become less linear.
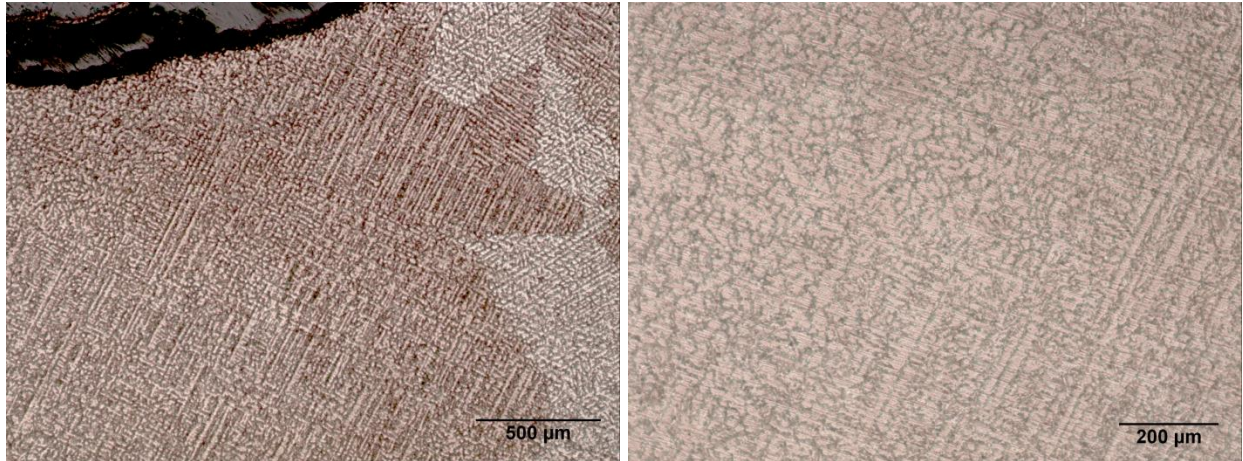
Figures 23a and 23b: Dendrites near loop of lion (50X), and as Site 3 approaches Site 2 from right to left (100X)

Site 4: SEM

SEM EDS analysis of Site 4 (Figures 24a and 24b) finally shows that the composition is reasonably consistent throughout the entire lion.

Map Sum Spectrum		
	Wt%	σ
Cu	65.0	0.1
Zn	31.0	0.1
Pb	1.7	0.1
Sn	1.1	0.1
Al	0.8	0.0
Fe	0.3	0.0
Si	0.1	0.0
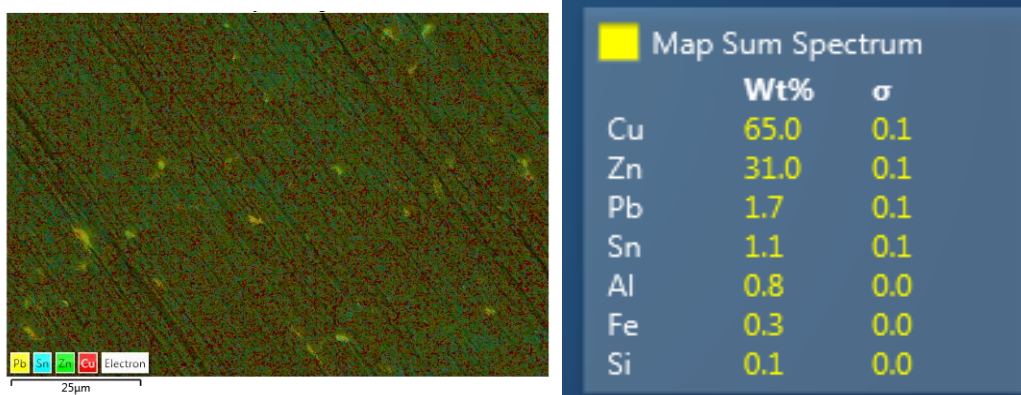
Figures 24a and 24b: Site 4 map sum data

Figures 25a and 25b show pores matching up to the dark purple areas seen on the tail end of the

microCT full body scans (see Figure 8a). They look similar to the porous area in the head and
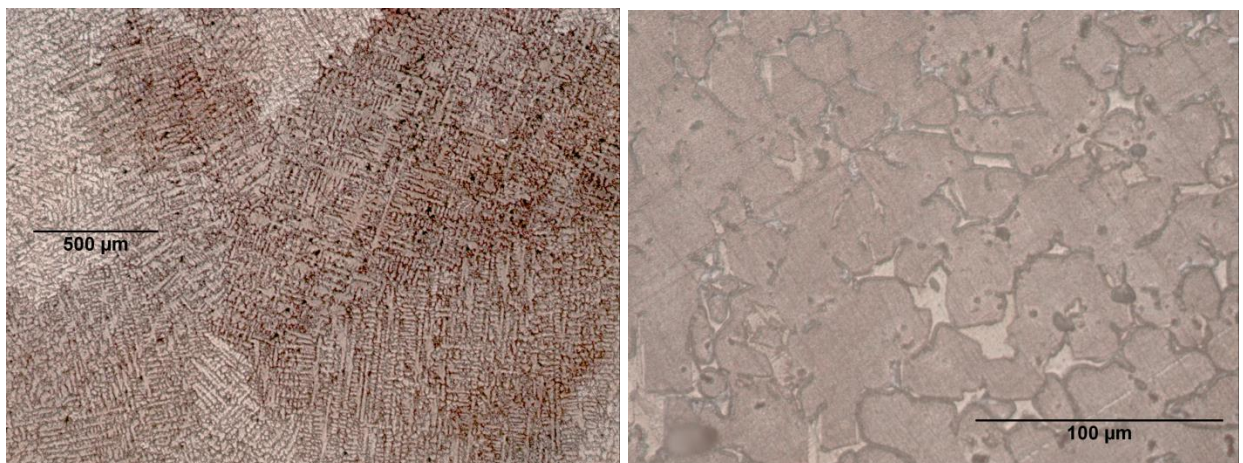
average around 50 microns long.
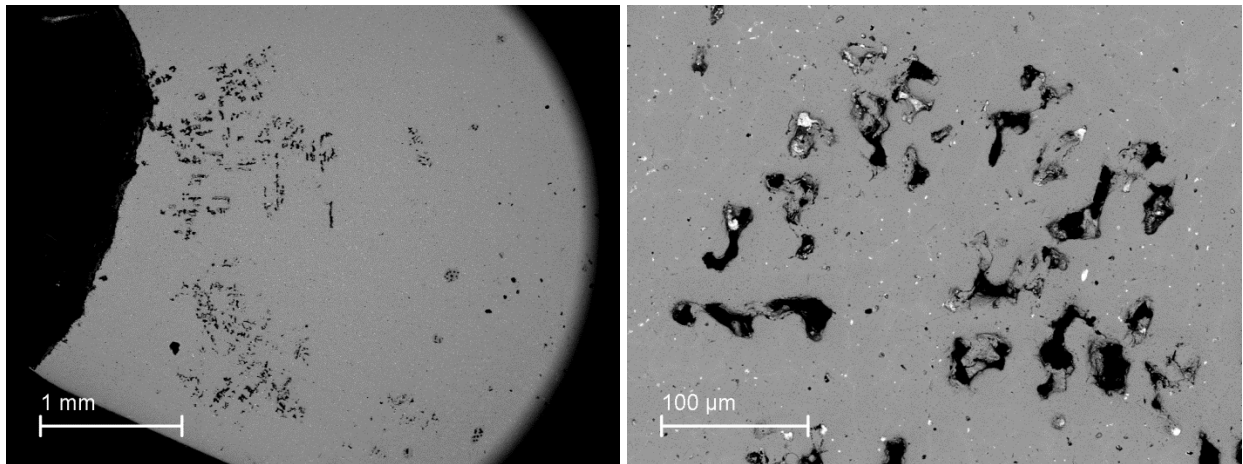
Figures 25a and 25b: Gas pores seen in the junction between the lion's hind legs

Site 4: Optical Microscopy

Figure 26a confirms that the general brass microstructure is preserved throughout the entire lion.

Figure 26b shows parts of the alpha and beta phases intermixing.

Figures 26a and 26b: Dendrites seen in the back end of the lion at 50X and 500X

X-ray Fluorescence

Below are the results of X-ray Fluorescence (XRF) conducted on the lion samples. They reaffirm

results obtained by the SEM-EDS, in that there is a significant amount of zinc present in the

sample. It is when the minor components are concerned that the results begin to differ from the

SEM. Figure 27 shows there to be very small amounts of nickel and almost negligible amounts

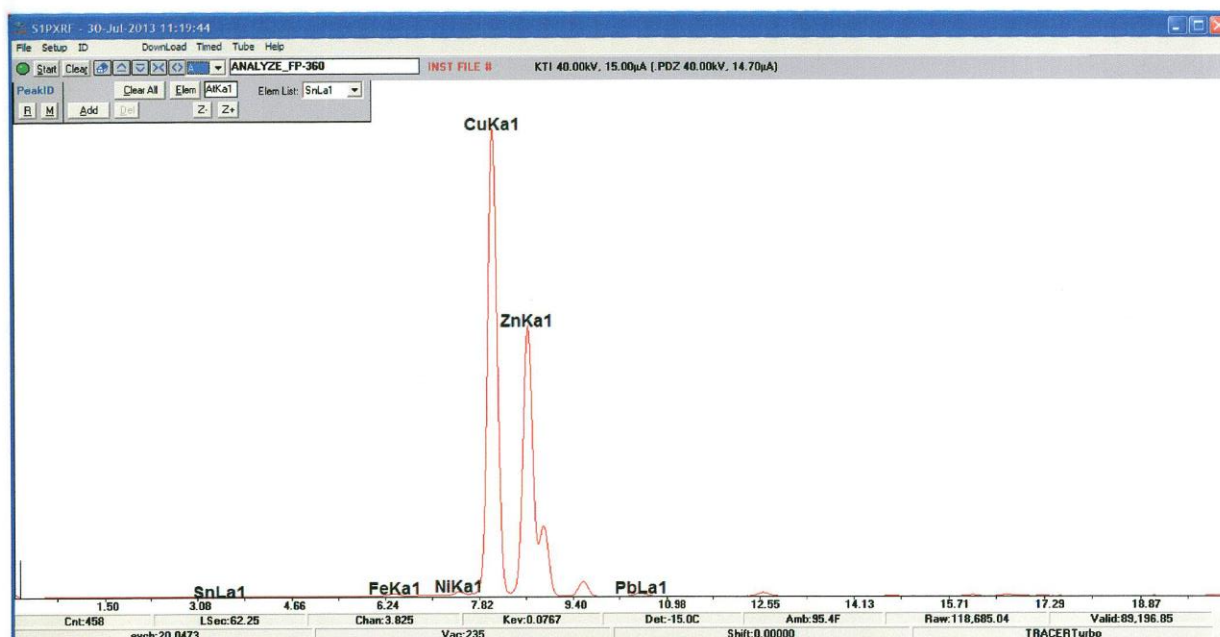of tin. Figure 28 shows there to again be nickel and no registered tin.

Figure 27: XRF results taken at Site 2, tin peak barely present
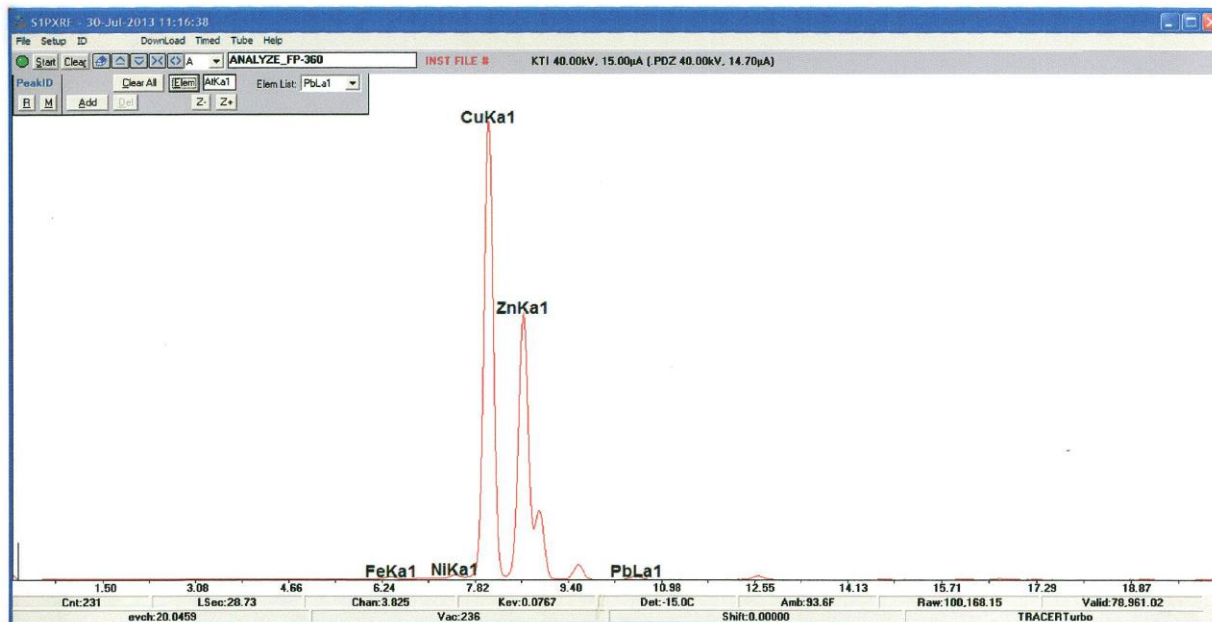
Figure 28: XRF results taken on Site 4, lead alpha and beta peaks equally as tall

Discussion

MicroCT

From the microCT alone, one cannot verify the authenticity of an artifact. There are a few internal features worth exploring in detail later, but nothing can be specifically confirmed from the list of stipulations provided on the certificate. This being said, the microCT is an excellent tool if the authenticity has already been verified and the integrity of the artifact is a concern.

Mold Making Process

It is known that artificial patinas will flake more readily than true ones, brought on by the fact that they are rapidly produced and do not have to weather hundreds of years of Mother Nature. Furthermore, Paul Craddock indicates that "shiny metal appearing on the edges and extremities of a patinated bronze is an indication of recent patination," in his book *Scientific Investigation of Copies, Fakes, and Forgeries*, as has been seen on the bottom corners of the lion legs.

Site 1

Because the material contains zinc and copper, not tin and copper as was expected, it can be concluded that the certificate of authenticity provided by the seller is inaccurate. Furthermore, historical research shows that ancient metalsmiths did not have the ability to create brass at concentrations exceeding the 28% zinc maximum that could be produced by smelting zinc and copper ores together[3]. Zinc metal was difficult to work with in ancient times because it would reach the vapor phase at temperatures below those required for extraction. As a result, the zinc would escape instead of combining with the copper ores.

The SEM will have some error. It is understood that 28% is close to the 31-32% measured in the SEM. This alone cannot rule out that the sample can possible still be Mesopotamian from 1200 BC.

However, when brass was popularized in ancient times, the zinc concentration was mostly far less than this 28% threshold. It is not until the late 1500's AD that Chinese civilizations began to produce brass at zinc concentrations greater than 30%, notably 2700 years after the artifact is claimed to have been made. Most brasses were accidental in the Bronze Age, the copper ore containing 5 to 15% zinc that was not removed during smelting[3].

The high percentage of chlorine in the corrosion layers (8-15%) indicates that the object was either soaked in saltwater or an artificial corrosion environment. A variety of methods could have artificially produced a dark brown inner corrosion layer and a green outer layer; based on EDS data, chlorine and iron were probably the chemicals used. The outermost layer of corrosion contains a very small percentage of zinc, suggesting that it was preferentially removed. The mechanism behind which generally suggests that zinc and oxygen migrate to the outside of the oxide layers, while copper does not[2].

Site 2

The SEM shows there to be a series of pores within the neck of the lion. These are probably the result of a casting defect; if gas bubbles could not escape, they would have segregated to the thickest part of the material as it was cooling. This says a lot about the skill of the metalsmiths. They were able to create a figure with details on the head, but they were not able vent the casting to prevent gas pores.

The location of these pores varies slightly according to which method of analysis was used. Figure 8b shows the porous area to be near the outer edge of the neck, while visual inspection of the sample shows the pores to be concentrated in the center of the neck not reaching toward the edges. This discrepancy should be taken into account when using the microCT for future studies.

Site 4

The pores seen in the SEM again explain the less dense region seen in the microCT. Looking back to Figure 25a, the left edge of the sample is the curve of the back leg. This shows that these pores are closer to the location indicated by the microCT than was seen with Site 2.

Forgeries

The lion was a symbol of aggression in Mesopotamian society because lions were threatening predators that traveled in packs. As a result, Mesopotamia also viewed the lion as a symbol of heroics, because they required great strength and skill to be defeated. Some of the most common relics from ancient times include pottery and cylinder seals that are decorated with animal/ human scenes. These include fighting amongst animals, animals and humans, and animal hybrids such as lion headed eagles that brought myths to life[6]. It is possible that the creator of this forged lion artifact took was inspired by these scenes and chose to replicate the lion because it was such popular imagery.

Conclusion

Because of the high zinc content in the lion, it is highly unlikely that it could be from Late Bronze Age Mesopotamia. It is more than likely a creation of modern leaded yellow brass meant to replicate figures that would have been popular among Mesopotamian society. Future uses of the microCT should take into account that it was an excellent investigative tool to nondestructively explore and predict the internal features of artifacts, but it could not have verified the authenticity of the artifact by itself and needed to be coupled with other methods of study.

Appendix 1: MicroCT

MicroCT Tomography

1. Open XMController, mount sample, stick on Stage
2. Select "lightbulb" icon, heat up to 80 kV (will read 0) when finished
3. Open "Visible Light Cam Ap" from Start menu
4. Position Source at -100 and Detector at +50, while Stage set at 0 for x, z, and theta
5. Switch objective to lowest resolution (0.39X)
6. Position sample roughly with joystick (so that target area is in field of view)
7. Close door and turn on X-Ray, kV set to 80 and power at maximum 10
8. Select continuous imaging for 1 second, binning probably at 2
9. Turn on axes by going to View and Highlight Center FOV (below last check)
10. Position ROI in center of view by double clicking on image
11. Center ROI in the +90 and -90 directions (stay along axis for second adjustment)
12. Switch to desired magnification using "magnifying glass" icon
13. Adjust position of Source (backward from -100) to ensure ROI is in field of view
    a. Fine tune axes again at +90, -90 if needed
14. Write down Y coordinate
15. Turn off x-ray, adjust theta until it can be confirmed at the sample will not wreck
16. Turn on x-ray, press "stop" icon
17. Adjust "two gears" icon to single, at 1 second
    a. Evaluate image counts, adjust time (10 seconds)
18. Calculate a/b ratio
    a. Take scan using "camera" icon (1 with sample in image, and 1 at Y=20,000)
    b. Via Process and "image calculator" match a/b ratio to chart
    c. Move up in kV if needed or select filter
    d. **If go out of view then in view, program goes in correct a b order
    e. Pg 97 indicates to increase kV to 150 if needed for transmittance
19. To get count as close as possible to >5000 adjust time
20. Acquire tomography points using Tomography Location tool
    a. Via View and "highlight center FOV"
    b. Tools -> select the square with the circle and X in it
    c. Match up axes with square circle X
    d. CLEAR EXISTING POINTS, ok
21. Set up Recipe
    a. Click the "add list" square button
    b. Under "Camera" set exposure time to previously determined quantity
    c. Minimum number of images must be start +end angle +1, however 1600 is ideal
    d. Two boxes under references read: 10, "1/4 of min number of images"
    e. SAVE AS under Rachel file with notes
22. Start

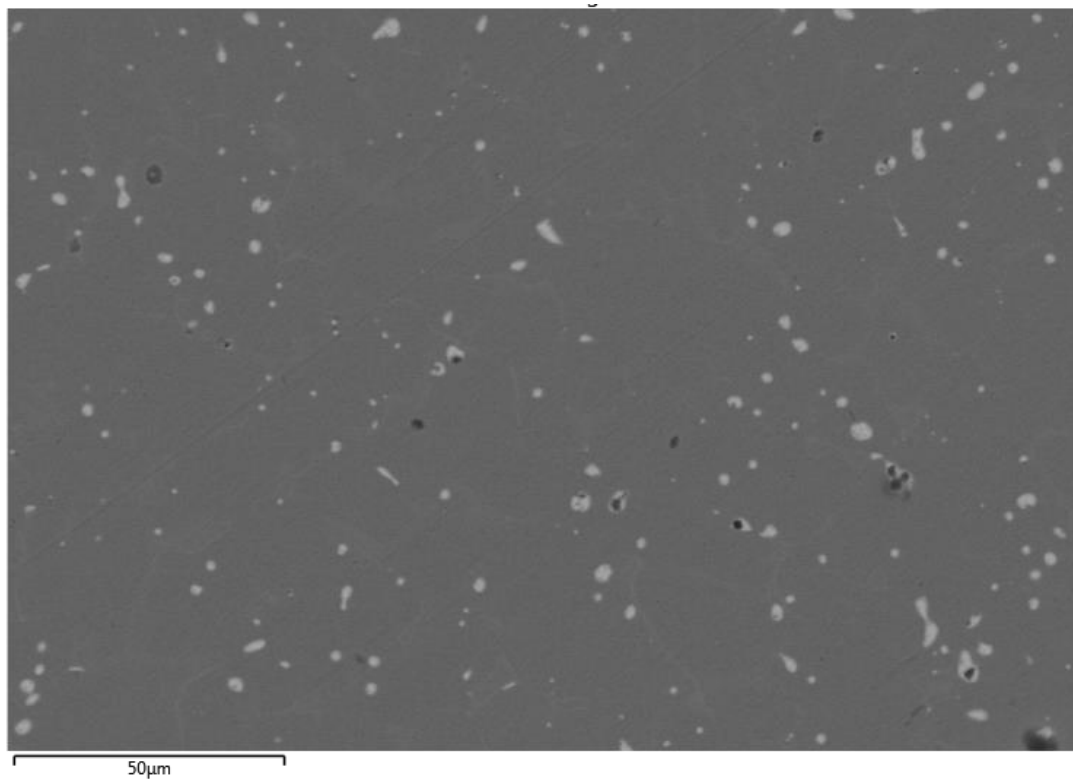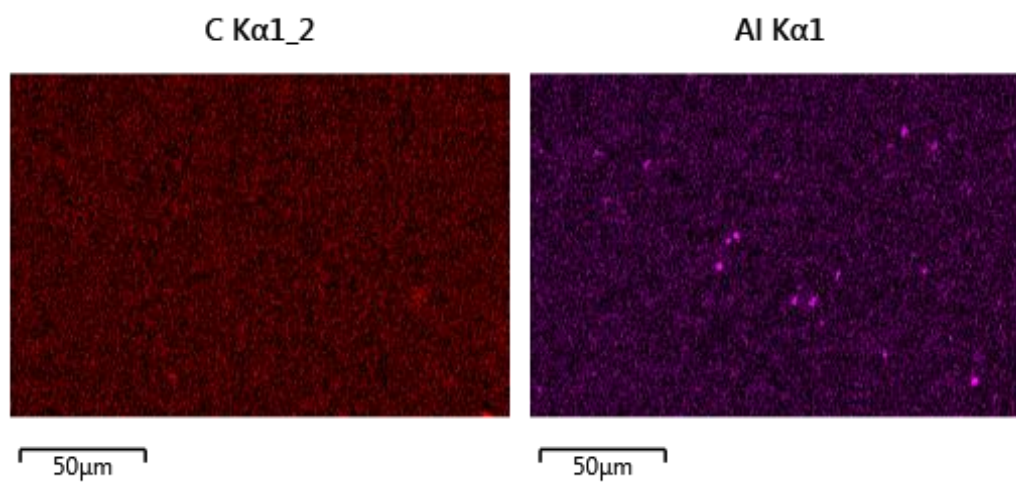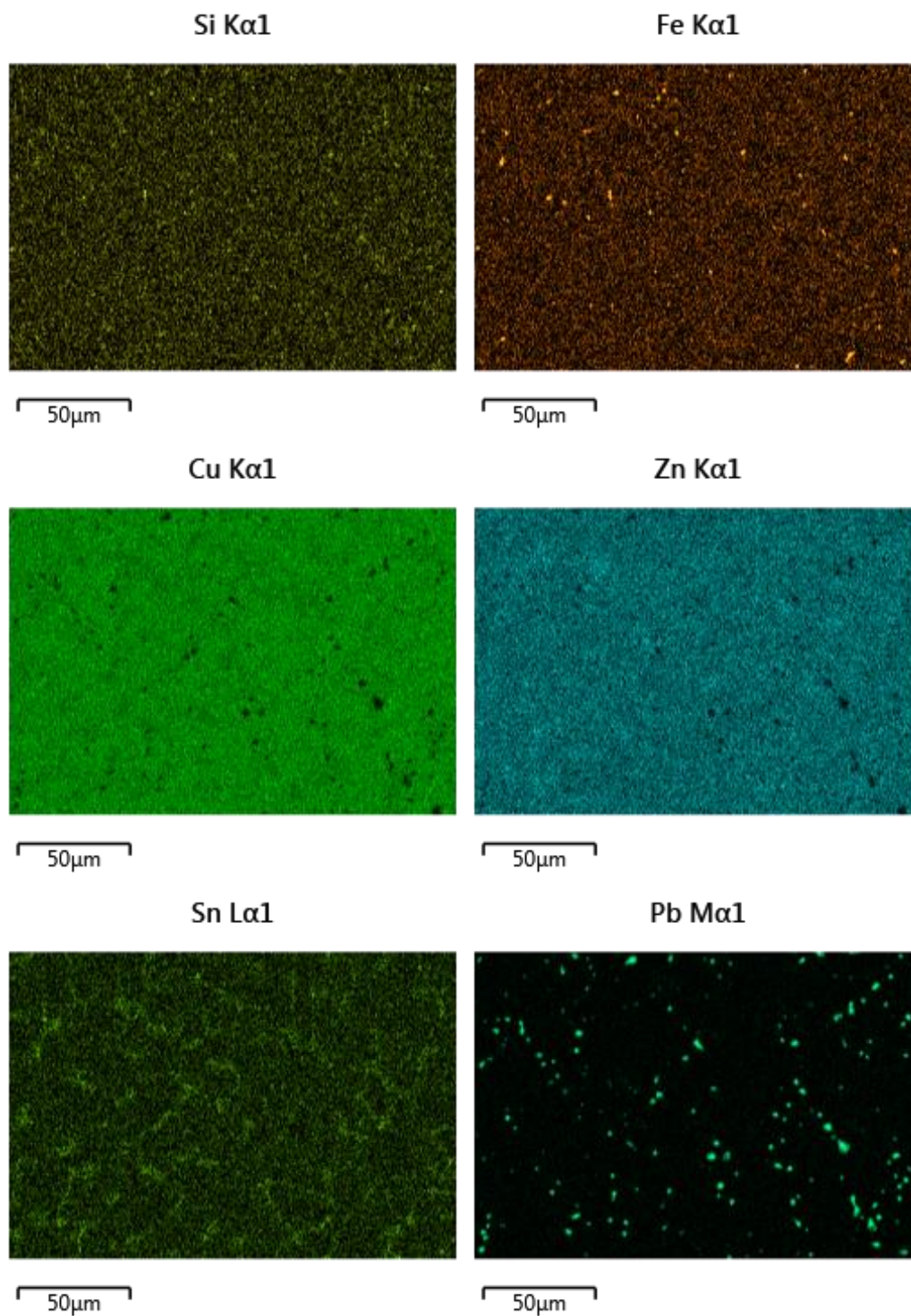# Appendix 2: SEM Figures

Site 1

Figure 29: SEM EDS electron image from bulk material of Site 1

Si Kα1

Fe Kα1

50μm

50μm

Cu Kα1

Zn Kα1

50μm

50μm

Sn Lα1

Pb Mα1

50μm

50μm

Figures 30: SEM EDS data of Site 1. Copper and zinc evenly distributed, tin in veins, lead in globules, and aluminum from polish in holes
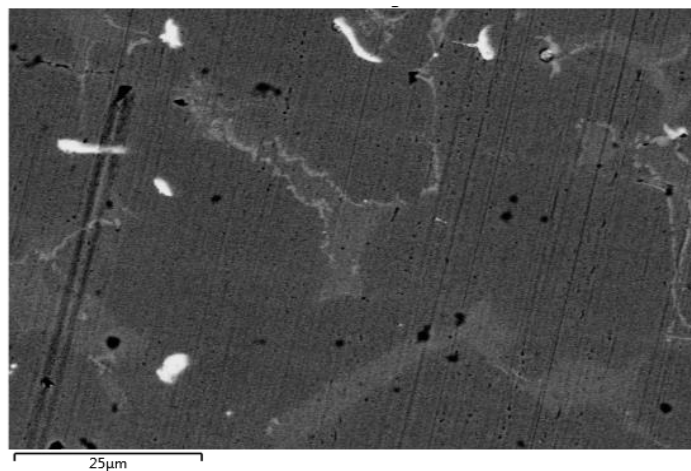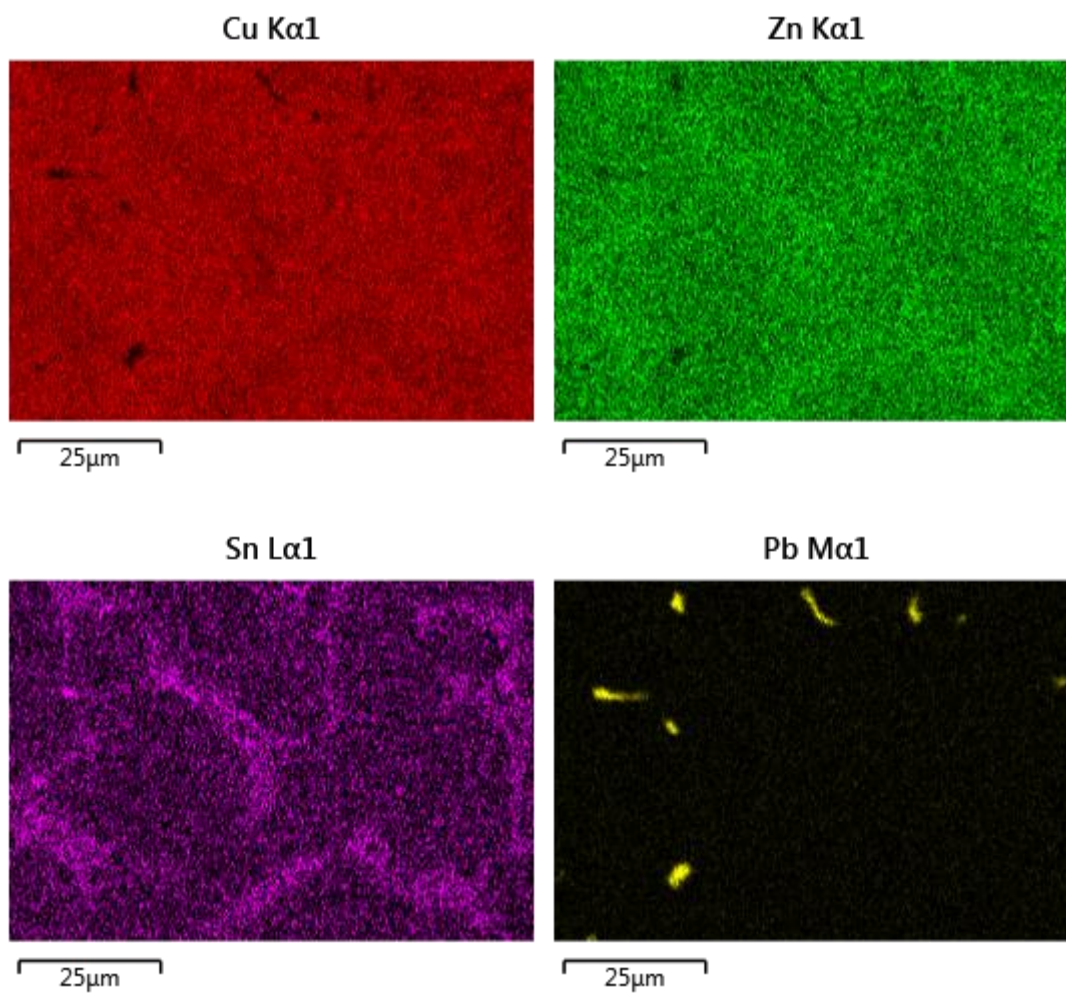
Site 2

Figure 31: SEM EDS electron image from Site 2

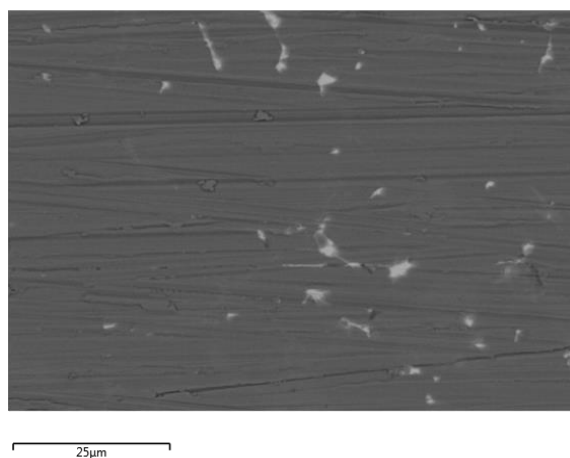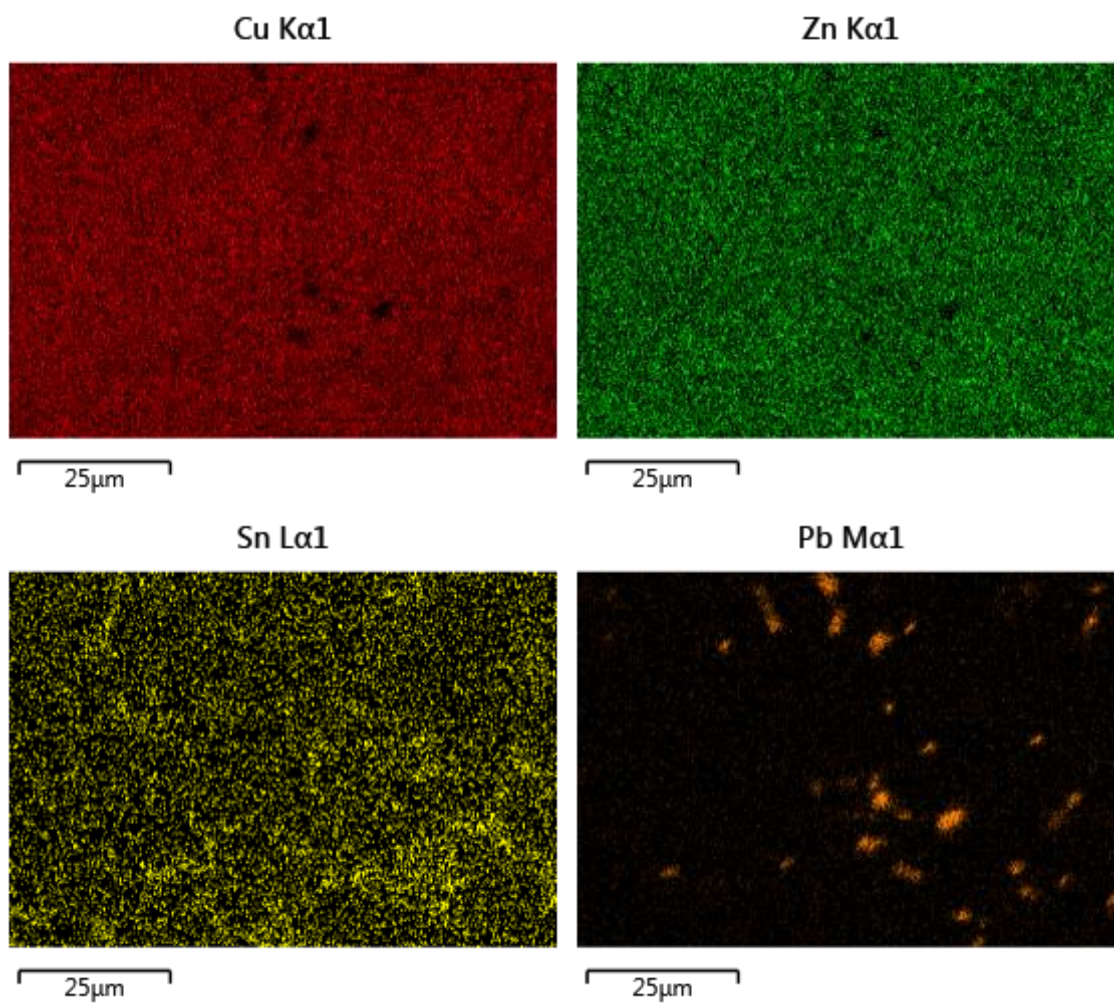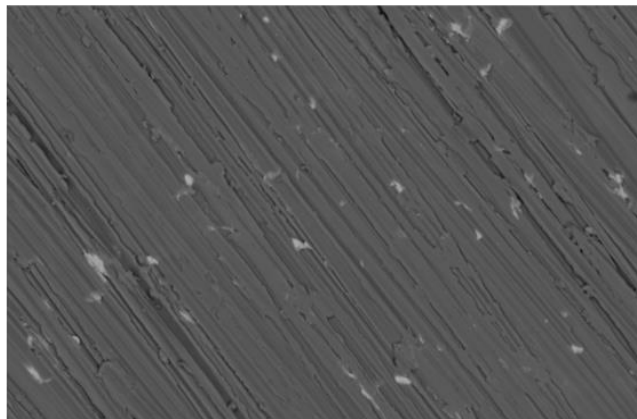Figures 32: SEM EDS data from Site 2. Similar behavior to Site 1.

Site 3

Figure 33: SEM EDS electron image of Site 3, only polished through 800 grit

Figures 34: SEM EDS data from Site 3, similar behavior to Sites 1-2

Site 4

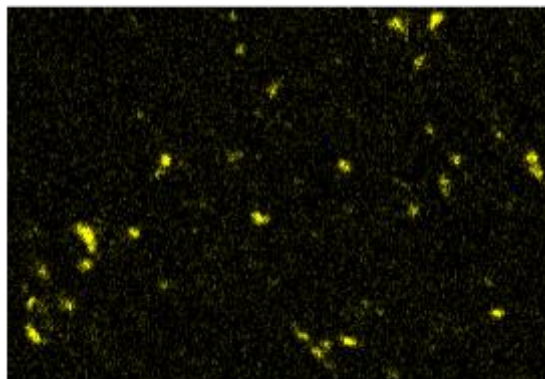Figure 35: SEM EDS electron image of Site 4, only polished to 800 grit
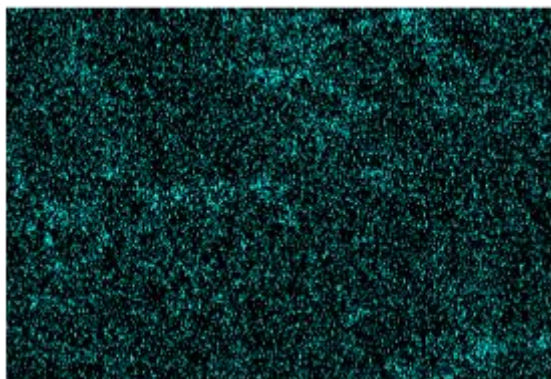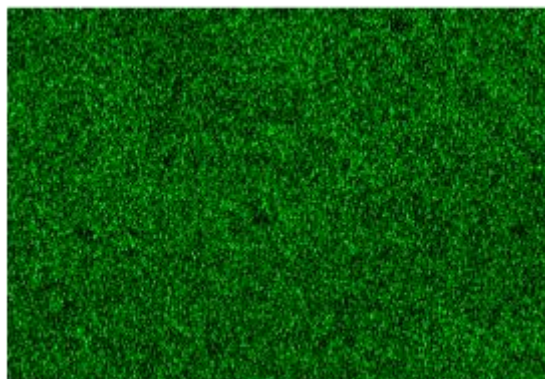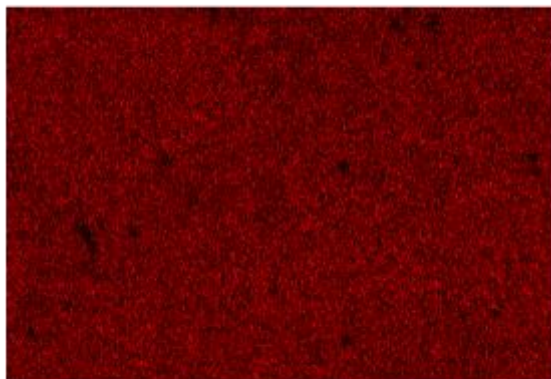
Figures 36: SEM EDS data from Site 4, exhibiting similar behavior to all Sites

Acknowledgments

References

1. Angelini, E., Batmaz, A., Cilingiroglu, A., Grassini, S., Ingo, G. M., & Riccucci, C. (2010). *Tailored analytical strategies for the investigation of metallic artefacts from the ayanis fortress in Turkey*. Informally published manuscript, Available from Wiley InterScience.

2. Barr, T. L., & Hackenberg, J. J. (1982). *Determination of the onset of the dezincification of &-brass using x-ray photoelectron (esca) spectroscopy*. Informally published manuscript, Available from American Chemical Society.

3. Craddock, P. (2009). *Scientific investigation of copies, fakes and forgeries*. Slovenia: Butterworth-Heinemann.

4. DeWitte, Y., Cnudde, V., Pieters, K., Masschaele, B., Dierick, M., Vlassenbroeck, J., & Van Hoorebeke, L. (2008). *X-ray micro-ct applied to natural building materials and art objects*. Manuscript submitted for publication, Department of Radiation Phyrics, Ghent University, Ghopfent, Belgium. Available from Wiley InterScience.

5. Galli, H., Knopf, R., & Gordon, R. (2007). *The aging of solder joints over 1,600 years: evidence from nubian bronze aftifacts*. Informally published manuscript, Department of Geology and Geophysics, Yale University, New Haven, Connecticut, Available from ProQuest. Craddock, P. (2009). *Scientific investigation of copies, fakes and forgeries*. Slovenia: Butterworth-Heinemann.

6. Goff, B. L. (1963). *Symbols of prehistoric Mesopotamia*. New Haven: Yale University Press.

7. Hughes, S. (n.d.). *CT scanning in archaeology*. Manuscript submitted for publication, Department of Physics, Queensland University of Technology, Brisbane, Queensland, Australia. Retrieved from www.intechopen.com.

8. Jansen, R. J., Poulus, R. T., Kottman, J., de Groot, T., Huisman, D. J., Stoker, J., & , (2006). *CT: A new nondestructive method for visualizing and characterizing ancient roman glass fragments in situ in blocks of soil1*. Manuscript submitted for publication, Department of Radiology, University of Amsterdam, Amsterdam, Netherlands. Available from RadioGraphics.

9. Pollard, A. M. (2009). What a long strange trip it's been: lead isotopes and archaeology. In A. Shortland, I. Freestone & T. Rehren (Eds.), *From Mine to Microscope* (pp. 181-190). Oxford, UK: Oxbrow Books.